

# Lab on a Chip

Accepted Manuscript



This is an *Accepted Manuscript*, which has been through the Royal Society of Chemistry peer review process and has been accepted for publication.

*Accepted Manuscripts* are published online shortly after acceptance, before technical editing, formatting and proof reading. Using this free service, authors can make their results available to the community, in citable form, before we publish the edited article. We will replace this *Accepted Manuscript* with the edited and formatted *Advance Article* as soon as it is available.

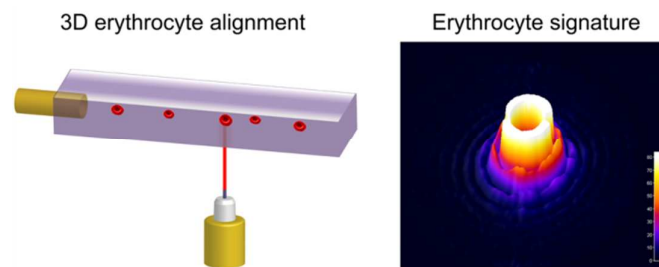
You can find more information about *Accepted Manuscripts* in the [Information for Authors](#).

Please note that technical editing may introduce minor changes to the text and/or graphics, which may alter content. The journal's standard [Terms & Conditions](#) and the [Ethical guidelines](#) still apply. In no event shall the Royal Society of Chemistry be held responsible for any errors or omissions in this *Accepted Manuscript* or any consequences arising from the use of any information it contains.

## Table of content for Lab on a Chip:

### Optical signature of erythrocytes by light scattering in microfluidic flows

Table of content:



Label-free analysis of individual erythrocytes, by a camera-based light scattering approach coupled with a viscoelasticity-induced cell migration in microfluidic flows.

## ARTICLE

# Optical signature of erythrocytes by light scattering in microfluidic flows

rrzCite this: DOI: 10.1039/x0xx00000x

D. Dannhauser,<sup>a</sup> D. Rossi,<sup>a</sup> F. Causa,<sup>b</sup> P. Memmolo,<sup>a,c</sup> A. Finizio,<sup>c</sup> T. Wriedt,<sup>d</sup> J. Hellmers,<sup>e</sup> Y. Eremin,<sup>f</sup> P. Ferraro<sup>c</sup> and P. A. Netti<sup>a,b</sup>.

Received 00th January 2012,  
Accepted 00th January 2012

DOI: 10.1039/x0xx00000x

www.rsc.org/

A camera-based light scattering approach coupled with a viscoelasticity-induced cell migration technique has been used to characterize morphological properties of erythrocytes in microfluidic flows. We have obtained light scattering profiles (LSP) of individual living cells in microfluidic flows over a wide angular range and matched them with scattering simulations to characterize their morphological properties. The viscoelasticity-induced 3D cell alignment in microfluidic flows has been investigated by bright-field and holographic microscopy tracking, where the latter technique has been used to obtain precise cell alignment profiles in-flow. Such information allows variable cell probability control in microfluidic flows at very low viscoelastic polymer concentrations, obtaining cell measurements that are almost physiological. Our results confirm the possibility of precise, label-free analysis of individual living erythrocytes in microfluidic flows.

## 1 Introduction

Blood plays an essential role in human health diagnostics, as its biochemical and cellular equilibrium is extremely sensitive to the variations occurring in the body at various disease stages.<sup>1</sup> Thus, a fast and accurate examination of blood cell properties is essential.<sup>2,3</sup> The gold standard for blood cell identification is the flow cytometer. Such a complex apparatus regularly performs optical and electrical analysis or sorting of individual cells, level of protein expression or lipids at high throughput rates (up to 10000 cells per s), typically requiring hydrodynamic sheath flow alignment and fluorescence antibody labelling.<sup>4,5,6</sup> Unlike such time-consuming and expensive fluorescence methods, advanced light scattering techniques can be used as fast label-free measurement system.<sup>7</sup>

In general, several optical inspection techniques based on tomographic or holographic approaches can be applied to characterize individual cells in-flow. The most relevant drawbacks of such techniques are their intrinsic complexity and computational costs. For instance, digital holography (DH) furnishes a light diffraction signature due to light passing through cells. The DH is able to perform quantitative multi-focus phase-contrast imaging by using numerical refocusing criteria.<sup>8-10</sup> Another system is the scanning flow cytometry (SFC), where a hydrodynamic sheath-flow focusing of cells is adopted. Combined with a coaxially arranged laser beam

interacting with a spherical concave mirror, the scattering range of the SFC is enhanced and measured by diverse PMTs.<sup>11,12</sup>

If the light scattering profile (LSP) is measured by a multi-element sensor, the overall complexity of most individual cell detection systems becomes greatly simplified.<sup>13</sup> In fact, continuous LSP collection over a large angular range can provide simultaneously all the morphological properties of an individual naive cell, e.g. shape, size, refractive index (RI) and orientation in relation to the direction of the incident light. Cell characterization can be processed significantly more simply, cost-effectively and faster when performed coupling continuous LSP measurements with individual cell interrogations in-flow.

Viscoelastic migration in microfluidic flows can be considered as a straightforward and promising method to align cells without applying any force external to the flow itself. Several alignment, sorting and classification devices for human blood cells have been published in the last years.<sup>14-18</sup> Nevertheless, to our knowledge, label-free characterization of living human blood cells by wide angle light scattering, combined with precise 3D viscoelastic alignment, does not exist yet. Investigations on non-spherical blood cells -such as erythrocytes- can be used to prove our concept.

In order to gain information from a light scattering approach, it is necessary to solve the non-trivial inverse-LSP. In principle, the LSP is fitted step by step to a simulation curve, reducing the variance of error until a suitable result is obtained.

Several publications regarding erythrocyte simulations for scattering approaches can be found in literature. For instance, time domain methods, such as the finite integration technique (FIT)<sup>19</sup> or the finite difference time domain (FDTD)<sup>20</sup> can be applied. Increasing interest can be noticed for the discrete dipole approximation (DDA), provided by Yurkin *et al.*<sup>21</sup>. Eremina *et al.*<sup>22</sup> showed the potential of a less CPU-intensive approach, based on the discrete sources method (DSM). In addition, the boundary element method (BEM) approach<sup>23</sup> or T-matrix method<sup>24</sup> can be applied to simulate the scattering effects of erythrocytes. Each of these methods has its advantages and disadvantages regarding CPU-usage and simulation accuracy. In this work we will not go into detail about differences between the above listed simulations methods; interested readers are referred to the work of Wriedt *et al.*<sup>19</sup>.

Here we present a direct way to investigate individual erythrocytes in microfluidic flows using a wide angle LSP approach. We applied the DDA and DSM simulation approaches to validate erythrocyte LSPs in microfluidic flows. Viscoelastic 3D cell migration -shown in our previous study for rigid latex particles<sup>25</sup>- was successfully applied to non-spherical living erythrocytes at diluted polymer concentrations. In order to verify cell alignment, we employed a DH method in combination with a white light standard microscope to 3D track erythrocytes in-flow. For our DH purpose, we successfully applied a refocusing method for the 3D tracking of living cells.<sup>26,27</sup>

## 2 Materials and methods

### 2.1 Sample preparation

For each measurement, 3 mL of blood from a healthy donor were taken, by standard venipuncture procedure, and stored in a K<sub>2</sub>EDTA tube (BD Vacutainer) preventing coagulation. Samples were analysed within two hours of collection at room temperature.

Cell concentration in microfluidic flow is a critical factor for light scattering and DH analysis, due to possible multiple cell interactions. In order to obtain a suitable number of erythrocytes, the blood sample was diluted 1 million times with the microfluidic medium consisting of Poly-Ethylene Oxide (PEO - M<sub>w</sub> = 4 MDa, SIGMA-ALDRICH) dissolved in a standard Phosphate-Buffered Saline (PBS, EUROCLONE). No glucose or other nutritious substances -which can scatter light- were added to the microfluidic medium, due to short experimental times. A pH and osmolarity of 7.4 and 286 mOsm/L, respectively, provided optimal cell conditions during our DH and light scattering measurements.

### 2.2 Cell observation

Cell vitality was controlled before and after each light scattering measurement with a Bright-field Microscope (BFM - X81 - OLYMPUS): a drop of pure blood was placed on a glass slide and observed with a 100x oil immersion objective.

We also performed Scanning Electron Microscopy (SEM - Ultra plus - ZEISS) observations to examine the morphological erythrocyte parameters needed for accurate light scattering simulations. Two drops of blood were placed in poly-L-lisine coated chambers, where platelets were activated by adding 0.2 mL of 0.2 M calcium chloride solution. Samples were subsequently fixed by adding 1 mL of 4% paraformaldehyde, 0.4% glutaraldehyde in 0.1 M sodium cacodylate buffer. After washing with cacodylate 0.1 M buffer and treatment with osmium tetroxide for 16 h, the samples were dehydrated with increasing ethanol-water solutions (30%, 50%, 70%, 80%, 96%, 100%). Finally, samples were dried by a critical point drier (EM CPD300 - LEICA), coated with a 7 nm gold film (208HR - CRESSINGTON) and observed with the SEM.

### 2.3 Cell alignment

Viscoelastic fluids show two different rheological characteristics under deformation, one related to the viscous fluid component, the other to the elastic solid behaviour. We measured the zero shear viscosity  $\eta_0$  of scaling PEO-PBS concentrations (0.00625 g/dl – 0.4 g/dl), with a stress controlled rheometer (MCR 302 - ANTON PAAR - double cuvette geometry). For such diluted polymer concentrations the longest relaxation time  $\lambda_t$ , considered as the main parameter for elastic fluid behaviour, cannot be measured with such a rheometer due to predominant inertia effects.

However, the general ability of cell alignment of a pressure driven viscoelastic flowing solution strongly depends on its elastic part. The cell alignment can be expressed by a dimensionless parameter  $\theta = \dot{\gamma}\lambda_t + \beta^2(L/r_c)$ , with  $\dot{\gamma} = (\Delta P r_c) / (8\eta_0 L)$  the average shear rate of the fluid,  $\Delta P$  the applied pressure,  $L$  the capillary length,  $r_c$  its inner radius and  $\beta$  the confinement ratio between cell radius and  $r_c$ .<sup>28</sup> Referring to a  $\theta$  “master curve” as indicated elsewhere<sup>29</sup>, we calculated the  $\lambda_t$  of all our PEO-PBS concentrations.

Other hydrodynamic effects -the Segré-Silberberg effect or the Saffman lift force- which could shift cells to a position different from the centreline, were not considered for our polymer concentrations, due to their minor alignment influence compared to the viscoelastic force.<sup>29,30</sup>

### 2.4 Light Scattering setup

We used a scattering apparatus -whose design and basic principle is shown elsewhere<sup>25</sup>- able to accurately measure LSPs of differently sized individual particles or cells in microfluidic flows. The obtained LSPs span from 2°-30° with an optical resolution of 0.1022°, enabling erythrocyte diameter distinction of at least 0.1  $\mu\text{m}$ , due to the effort of the implemented narrow incident laser beam collimation ( $\lambda = 632.8$  nm) and optimized scattered light collection system.

A variable cell throughput up to 1.2 cells per s was obtained and analysed by a self-written Matlab routine to acquire unknown living cell properties.

### 2.5 LSP acquisition and simulation

Each scattered light collected by a pixel of the camera sensor was mapped to a corresponding magnitude of scattering wave-vector, as shown in our previous work<sup>25</sup>. The average scattering intensity of each scattering angle was combined to a continuous LSP and characterized by matching the best fitting individual cell simulation. To obtain the morphological erythrocyte properties we had to solve the inverse-LSP by calculating possible theoretical erythrocyte scattering profiles.

Erythrocytes are biconcave disks enclosed by a thin, elastic, lipidic bi-layer of around 7 nm. A mature erythrocyte is a soft, flexible and elastic cell, which has neither nucleus nor substantial internal elements. It is composed of a membrane (3% - RI = 1.3317), water (65% - RI = 1.3317) and haemoglobin (32% - RI = 1.6150).<sup>31</sup> In literature, reported RIs of erythrocytes vary in a range from 1.4000 to 1.4600 for the real part, primarily related to the haemoglobin concentration, while the imaginary part can be neglected.<sup>15,31,32</sup> In an isotonic saline solution, human erythrocytes range between 6-9  $\mu\text{m}$  in diameter, with a mean value of around 7.65  $\mu\text{m}$  and a thickness of 1.42-2.84  $\mu\text{m}$ .<sup>33</sup> Also, erythrocytes with a diameter greater than 9  $\mu\text{m}$  (macrocytes) or smaller than 6  $\mu\text{m}$  (microcytes) can be found in human blood.<sup>15</sup> It is worth knowing that the isotonicity between medium and erythrocytes is a critical parameter for light scattering approaches. The physiological osmolarity value for erythrocytes is defined to be circa 290 mOsm/L, whereas in an hypotonic medium (<290 mOsm/L) cells tend to swell, while shrinkage can be observed for hypertonic conditions (>290 mOsm/L).<sup>34</sup>

We used a surface and a volume based simulation method to solve inverse-LSP. The DDA method (ADDA v1.2) approximates the scatterer by a lattice of dipoles, using a spacing between the dipoles smaller than the laser wavelength. In general, the dipole number depends on numerical accuracy, geometry of the cell and RI. The dipoles have an oscillating polarization in response to both the incident plane wave and the electric fields. DDA is a robust simulation approach applicable to a wide spectrum of cell shapes.<sup>21</sup>

We also implemented a surface based method using a semi-analytical DSM approach. Such a method uses an approximate solution, which is constructed by representing the electromagnetic fields as a finite linear combination of the electric and magnetic fields of multi-poles distributed inside the scatterer. DSM combines fast computational speed with the ability to calculate light scattering for any directions of incident light at the same time. In the case of erythrocytes, discrete sources are deposited in a complex plane flanked to the symmetry axis of the particle.<sup>19</sup> In general, relatively fast calculation times compared to DDA, at similar scattering results are obtained for DSM simulations.<sup>19,35</sup>

Our scattering apparatus provides measurements of un-polarized scattered light. In fact, only the  $S_{11}$  element of the Mueller matrix (obtained by the ADDA software) -or the average value from parallel and perpendicular scattering plane from the DSM simulation- was used, providing un-polarized individual cell scattering.

## 2.6 Holographic setup

DH in microscopy is a well-established imaging technique for the investigation of cells motility.<sup>8-10</sup> In particular, we exploited the ability of DH to retrieve the axial positions of imaged cell with the aim to investigate erythrocyte alignment along the optical axis. We used a classical DH microscope with a DPSS laser ( $\lambda = 532 \text{ nm}$ ) as a light source, whose beam is coupled to an optical fibre (SF). The fibre splits the incoming laser light into object-beam and reference-beam. The object-beam impinges on the sample (S, i.e. the microfluidic chamber) before being collected by a 20x objective (MO). A CCD camera (UI-3370CP – IDS) with 512x2048 pixels (size 5.5 x 5.5  $\mu\text{m}^2$ ) is placed at a proper distance from the image-plane produced by the imaging objective; the CCD plane collects digital holograms at 100 fps through a beam-splitter (BS) and the imaged field of view is 50x200  $\mu\text{m}^2$ . A sketch of our setup is reported in Figure 1.

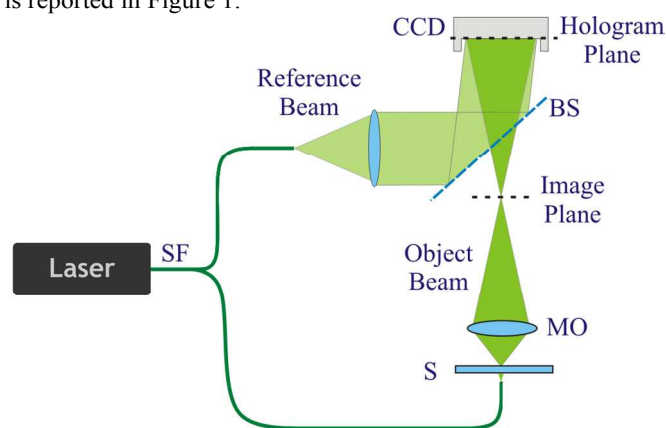


Fig. 1: Sketch of the holographic setup. The light source is coupled to an optical fibre (SF), which splits the laser light into object- and reference-beam. The object-beam impinges on the sample (S) before both beams are collected by the CCD camera.

Each holographic sequence is numerically processed; optical axis positions of all cells, passing the imaged field of view are retrieved by using a suitable refocusing criterion, based on the Tamura coefficient (TC) method.<sup>26,27</sup> Such analysis is based on amplitude reconstructions of recorded holograms, in which cells appear in-focus when  $TC = [\sigma_I/\mu_I]^{0.5}$  is minimized, with  $I$  the amplitude image,  $\sigma_I$  and  $\mu_I$  the image gray-level standard deviation and mean, respectively.

## 3 Results and discussion

### 3.1 Cell observation

The precise erythrocyte measurement via light scattering needs preliminary assumptions of morphologic parameters. We exploited SEM images from a proband to define the cell shape of a naive erythrocyte. (see Fig. 2a) An average erythrocyte diameter of  $6.91 \pm 0.63 \mu\text{m}$ , with a minimum ( $b$ ) and maximum ( $h$ ) cell thickness of 1.15 and 1.92  $\mu\text{m}$ , respectively, was measured for 57 cells and used as an input for our LSP simulations model (see Fig. 3b).

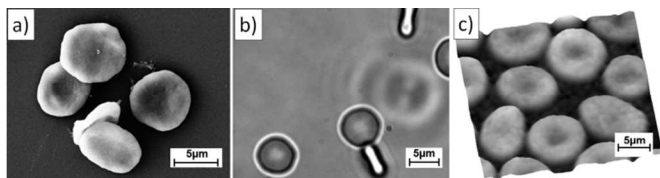


Fig. 2: SEM, BFM and DH observation of erythrocytes. a) SEM example of cell shape and size. b) A BFM observation in PEO-PBS 0.2 g/dl solution. c) Pseudo 3D quantitative phase image obtained by numerical reconstruction of DH images.

Right before each scattering measurement, detailed cell observations -in viscoelastic medium- were obtained using a BFM (see Fig. 2b). Such a monitoring provides important information about cell vitality in respect to the used viscoelastic polymer. Note that a non-isotonic balance between cells and surrounding medium (hypotonic or hypertonic condition) can be easily noticed in such a procedure. After each measurement cells were observed again by the BFM, showing no significant deformations or evident morphological modifications (see Fig. S1c). The pixel aspect ratio of the camera was used to analyse 25 cells of each proband, resulting in cell diameters spanning from 5.9 up to 8.6  $\mu\text{m}$ . (see table 1) Furthermore, quantitative phase images were reconstructed from holographic recordings to control cell vitality and deformations in microfluidic flows (see Fig. 2c).

### 3.2 3D alignment measurements

Before performing light scattering measurements of individual erythrocytes, it is necessary to investigate cell alignment precisely. We measured the transverse ( $y$ -axis) and optical axis ( $z$ -axis) alignment of erythrocytes flowing in our microfluidic device for varying PEO-PBS concentrations.

A camera based cell tracking method with following measuring conditions was set:  $r_c = 25$  mm,  $L = 40$  mm, chamber profile of  $w = 381$  mm and  $h = 400$  mm,  $\Delta P = 1000$  mbar (see Fig. 3a).

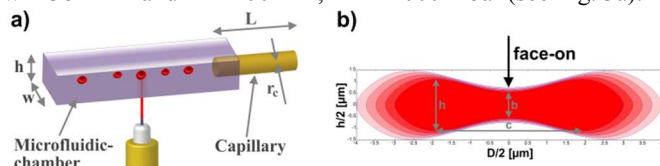


Fig. 3: a) Illustration of the microfluidic device. The round capillary enters the microfluidic chamber from the side, providing 3D particle alignment along the central axis. b) Erythrocyte cross-section of the scattering model for our DDA simulations for varying cell diameters (6-8  $\mu\text{m}$ ).

The microfluidic device was placed on a BFM with 20x objective, using a high sensitive CCD-camera (C11440-22CU - HAMAMATSU PHOTONICS) for data acquisition. At a free chosen position (5 mm after capillary outlet) a minimum of 100 cells, for alternating PEO-PBS concentrations, were recorded while passing a 94.5  $\mu\text{m}$  wide area defined as  $m$  (see Fig. 4a). The frequency distributions of the tracked erythrocytes are plotted in Fig. 4b.

The highlighted green areas in Fig. 4b (12  $\mu\text{m}$  wide) represent the fraction of perfectly aligned cells, important for precise scattering measurements. Our tracking routine automatically excludes all cells out of the focal plane (15  $\mu\text{m}$  wide  $z$ -axis

zone). As expected, reduced cell alignment with smaller PEO-PBS concentration and *vice versa* was observed. Similar data distributions can also be obtained for higher as well as lower  $\Delta P$  rates (data not shown).

Precise  $\lambda_r$  measurement of diluted polymer solutions is challenging<sup>30</sup>. By measuring the percentage of perfectly aligned cells, it is possible to relate their fraction to  $\theta$  and calculate the  $\lambda_r$  of the medium. (see Fig. 4c) We cannot claim to achieve precise  $\lambda_r$  values, since  $\theta$  is generally defined for rigid particles. We find that our  $\lambda_r$ -trend is in good agreement with literature values,<sup>32</sup> even though a small absolute shift can be noticed. Comparison with  $\eta_0$  measurement show similar trends (indicated in blue) for diluted (D) polymer solutions ( $D - x^1$ ) providing optimal measurement conditions for living cells. For higher polymer concentrations, where the physiological cell environment is not ensured anymore, the viscoelastic medium passes into the semi-diluted (SD) regime ( $SD - x^2$ ) before reaching the entangled (E) one ( $E - x^{3,4}$ ).

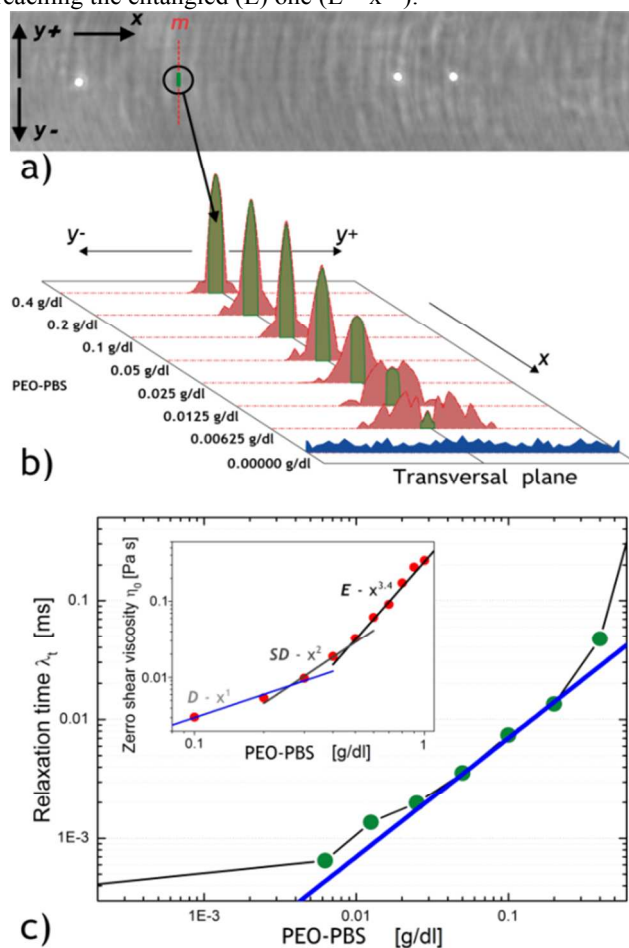


Fig. 4: Erythrocyte alignment testing for the transverse plane at varying PEO-PBS concentrations. a) Cells flowing ( $x$ -direction) in the microfluidic chamber (image view is 136.5x665.6  $\mu\text{m}^2$ ), with  $m$  the measurement plane ( $y$ -direction). b) Frequency distribution of cells at changing polymer concentrations. Green area indicates the fraction of cells precisely flowing in the transverse centreline. c) Calculated  $\lambda_r$  vs. polymer concentration with  $\eta_0$  obtained by rheological measurements.

Yang *et al.*<sup>29</sup> show improved cell alignment of naive erythrocytes compared to stiff erythrocytes of the same size, for

a highly concentrated viscoelastic medium. We confirm this behaviour with our measurements and find good agreement between  $\lambda_i$  values and observed cell alignment for strongly diluted polymer solutions. Our results indicate reliable cell alignment for PEO-PBS concentrations down to 0.025 g/dl in cell solution conditions similar to physiological ones, highly desirable for individual cell analysis.

In addition to the transversal alignment, we studied the orientations of the flowing cells. At position  $m$ , more than 97% of the observed erythrocytes were transversally oriented. Thus, results allowed us to assume a constant erythrocyte orientation at  $m$ , simplifying LSP simulations to an incident light angle of  $0^\circ$  (face-on orientation relative to the direction of the incident laser beam). (see Fig. 4a) Such erythrocyte orientation obtains more significant LSP results compared to higher incident light angles and is generally preferred.

In order to check the alignment along the z-axis, holographic sequences of erythrocytes in-flow were acquired by transmission configuration, fixing the PEO-PBS concentration at 0.2 g/dl and varying  $\Delta P$  (1000 and 3000 mbar). Fig. 5 reports an example of holographic refocusing using the TC method for an individual erythrocyte with corresponding insets showing in-focus and out-of-focus holographic reconstructions.

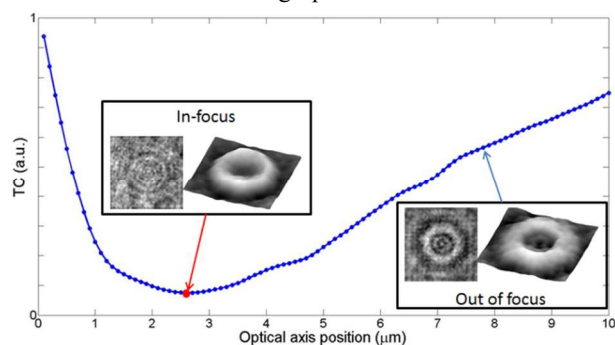


Fig. 5: TC refocusing criterion for an individually imaged cells. The minimum of TC is equal to the in-focus plane of RBC, i.e. its position along the z-axis.

The erythrocyte appeared in-focus at 2.6  $\mu\text{m}$  from the centre of the microfluidic chamber, indicated by zero. Each cell of the two recorded sequences was tracked in the imaged field of view; the average position along the z-axis and the corresponding standard deviation were evaluated. We report these results in Fig. 6, where the normal Probability Density Functions (PDFs) are evaluated by using the calculated average and standard deviation values.

As expected, the z-axis position measurements show well-focused results in the case of  $\Delta P = 3000$  mbar, as demonstrated by comparing the two standard deviations ( $\sigma_{1000} > \sigma_{3000}$ ). In addition, the comparison of their average values shows a significant z-axis shift from the centreline of the microfluidic chamber for the sequence recorded with  $\Delta P = 1000$  mbar ( $z_{1000} = -20.8 \mu\text{m}$ ).

This result is related to the effect of the gravity force that becomes dominant at lower flow velocities, limiting the effectiveness of the microfluidic focusing along the z-axis. In order to overcome this issue, a suitable  $\Delta P$  level for given

polymer concentrations is needed to guarantee an accurate 3D alignment of flowing erythrocytes over long measurement distances. In fact, our investigation leads to establish a  $\Delta P$  value equal to at least 3000 mbar at a given PEO-PBS concentration of 0.2 g/dl to provide minimum cell variance in-flow. Such high cell velocity results in perfect alignment with small variance over long microfluidic flow distances, for both the y and the z-axis trajectories.

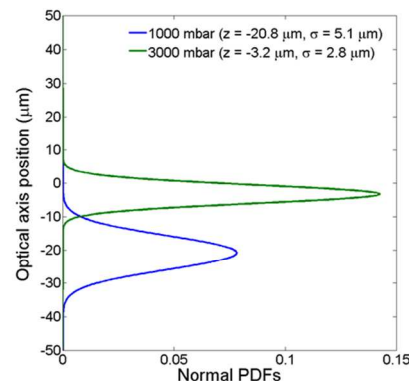


Fig. 6: Normal PDFs for two sequences of flowing erythrocytes, measured with different pressures ( $\Delta P = 1000$  and  $3000$  mbar).

However, a reasonable compromise between cell velocity and alignment variance should be set, to avoid possible cell deformations in-flow and respect the performance limitation of the used measurement system.

### 3.4 Light Scattering measurements

All light scattering measurements were performed at room temperature, with the previously described microfluidic device (see Fig. 3a). We used a PEO-PBS concentration of 0.2 g/dl and a  $\Delta P$  of 1000 mbar, resulting in suitable aligned cells at a velocity of  $100 \mu\text{m s}^{-1}$ . Such an erythrocyte velocity allows an achievable data acquisition configuration and avoids possible cell deformations in-flow, occurring at high  $\dot{\gamma}$ -rates. In view of the previously mentioned alignment results, our scattering apparatus was calibrated to the z-axis position of the used  $\Delta P$  value before each measurement, ensuring optimal microfluidic flow conditions. Note that acquisitions at higher  $\Delta P$  values, resulting in even smaller cell variances in microfluidic flow, are limited by the camera performance.

To obtain unknown morphological erythrocyte properties we had to solve the inverse-LSP. We calculated theoretical LSP from 5 up to  $10 \mu\text{m}$  in diameter, with a relative RI (rRI) of 1.0513 for the DDA and DSM-method; we used the Fung *et al.*<sup>33</sup> shape model and an extension of the Kuchel *et al.*<sup>35</sup> shape model, respectively. We do not claim that the used shape models are the best fitting ones for all measured erythrocytes; it is just a convenient and broad parameterization, which produces realistically looking shapes (see Fig. 3b).<sup>36</sup>

LSP simulation changes due to different erythrocyte shapes - calculated by the DSM and DDA approach- are shown in Fig. 7. The SEM parameters for DDA simulations were used with 0.250 (h/D), 0.170 (b/D) and 0.500 (c/D), according to the definition of Fig. 3b, while for the model of Fung *et al.* (0.370

0.187 0.638)<sup>33,37</sup>, as well as Kuchel *et al.* (0.275 0.125 0.625)<sup>35</sup>, literature parameters were used.

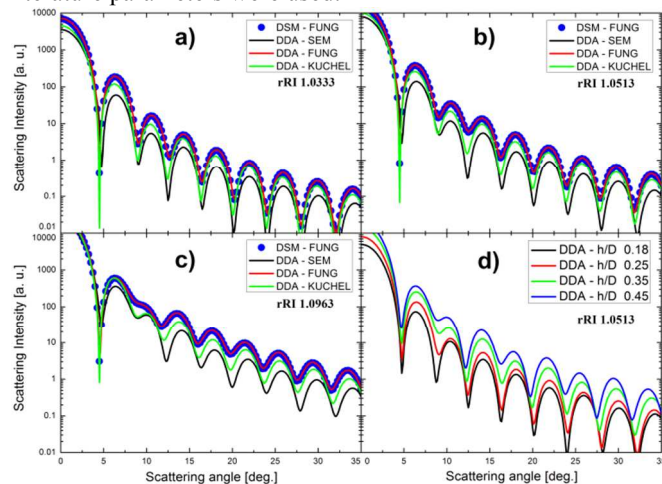


Fig. 7: LSP simulations (DSM and DDA approach) for our scattering apparatus at varying input parameters. Plot a), b) and c) show the rRI influence on the LSP simulation for different erythrocyte models (SEM, FUNG, KUCHEL), while in d) the influence of the cell thickness is highlighted. All curves are plotted for a cell diameter of 7.5  $\mu\text{m}$ .

We observed that by alternating the rRI in the range from 1.0333 up to 1.0963 and the cell thickness from 1.35 up to 3.37  $\mu\text{m}$  at a given cell diameter of 7.5  $\mu\text{m}$ , an absolute LSP intensity shift occurred, without effectively influencing the LSP oscillation form, as seen in Fig. 7d. DSM and DDA simulations calculated with the Fung *et al.* model showed equivalent LSP curves until the size of 10  $\mu\text{m}$  for our scattering range (data not shown). Such a perfect matching between both simulation techniques -with equal erythrocyte shape models- for LSP curves from 5 up to 10  $\mu\text{m}$  has not been published yet in literature and proves the validity of both simulation approaches. Erythrocytes for each proband were characterized, where one exemplary LSP for each proband overlaid by its corresponding simulation curve for DSM (Fung-shape) and DDA (SEM-shape) simulation is shown in Fig. 8.

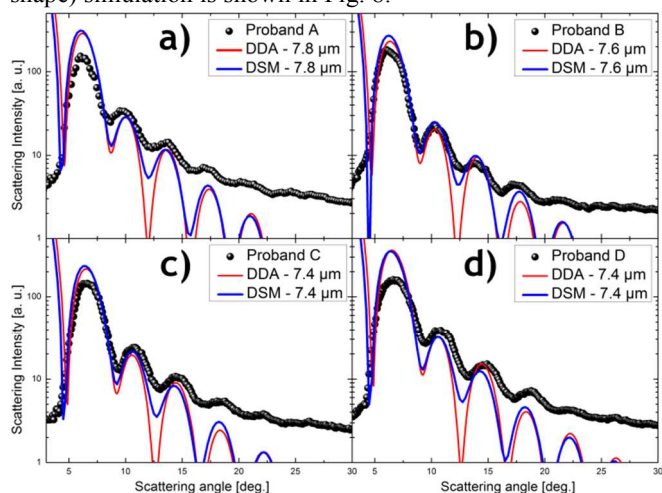


Fig. 8: LSP of an individual erythrocyte for each proband, obtained by our scattering apparatus. The red line illustrates the scattering simulation based on DDA simulations.

The minor LSP difference between the simulation approaches is due to the different erythrocyte shapes. Each LSP was matched with all pre-calculated simulation curves for both simulation approaches to obtain the best fitting one. No significant differences between the two simulation approaches were recognized. The LSP analysing procedure was focused to best match the angular section from 5-20°, due to the more significant scattering oscillations in this range. The minima and the maxima positions of each oscillation curve were taken into account to classify the best matching pre-calculated LSP curve. In case of mismatching among all simulations, the LSP was excluded from data analysis. In addition, an asymmetric erythrocyte shape measurement can provoke a noisy LSP and - in the worst cases- also blur individual oscillation structures, leading to its exclusion.

Indeed, in view of the minor influence of rRI and cell thickness on the LSP oscillation form -for our measurement conditions- the erythrocyte diameter remained the only significant parameter for precise LSP characterizations. The average diameter of an erythrocyte population, together with its variance, can be easily referred to the clinically measured 'Red blood cell Distribution Width' RDW-value<sup>1</sup>, giving useful information about the health status of a patient. We summarized the average erythrocyte LSP and BFM diameters in table 1.

**Table 1** Erythrocyte cell diameters (in  $\mu\text{m}$ ) reported for light scattering (LS combines DDA and DSM) and Bright Field Microscope (BFM) measurements. The p-value shows the results obtained from t-test comparisons between the two measurement techniques.

Proband	Age	Sex	Num.	LS - Dia.	Num.	BFM - Dia.	p-value
A	26	F	93	7.65 $\pm$ 0.44	89	7.29 $\pm$ 0.46	<0.01
B	31	F	93	7.76 $\pm$ 0.41	97	7.29 $\pm$ 0.64	<0.01
C	31	M	111	7.56 $\pm$ 0.59	88	7.34 $\pm$ 0.50	<0.01
D	30	M	110	7.57 $\pm$ 0.61	88	7.20 $\pm$ 0.51	<0.01

In fact, good agreement between measured and simulated LSPs were obtained, allowing precise living erythrocyte measurements in microfluidic flows. A healthy erythrocyte diameter typically lies between 6 and 9  $\mu\text{m}$ . Diameters obtained by our light scattering apparatus ( $\sim$ 7.64  $\mu\text{m}$ ) were generally slightly larger compared to BFM observations ( $\sim$ 7.28  $\mu\text{m}$ ). Such a small discrepancy can be associated to the applied LSP acquisition technique, which in our case is based on scattering symmetry. The results were analysed using the t-test, showing p-values below 0.01 making data comparison possible.

All cell diameters of each proband, obtained by our light scattering apparatus and analysed by matching the best fitting simulation method, are graphically summarized in Fig. 9. We found the majority of the measured erythrocytes between 7 and 8.3  $\mu\text{m}$  in diameter, which is in good agreement with values found in literature.<sup>19,31,33</sup> Proband A and B show a narrower diameter distribution compared to the other probands, while slightly higher average diameters are noticed.

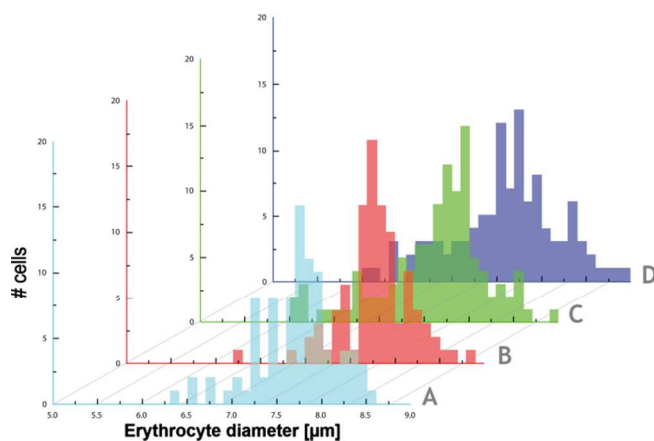


Fig. 9: Erythrocyte diameter distribution measured in microfluidic flow by our light scattering apparatus. The histogram a) and b) show female probands, while in c) and d) male probands are presented.

## 4 Conclusions

We have presented an accurate, straightforward, label free light scattering analysis of individual erythrocytes in microfluidic flows. Our analyses are possible due to the precise 3D alignment of individual cells taking advantage of viscoelasticity effects in strongly diluted PEO-PBS solution. It is important to note that -for the first time- low concentrations of PEO are adopted for 3D microfluidic alignment. PEO is an inexpensive, biocompatible and non-toxic commercial polymer.

Our measured LSP are matched with predicted DSM and DDA simulation profiles solving the inverse-LSP and obtaining the unknown erythrocyte dimensions. For the first time perfect LSP agreement from 5 up to 10  $\mu\text{m}$  in erythrocyte diameter between the two simulation approaches has been found. Diameter values from four different donors show a size value between 7 and 8.3  $\mu\text{m}$ , with an overall average value of  $\sim 7.64 \mu\text{m}$ , which is in good agreement with literature values. Our results demonstrate the ability of a rapid and cost-effective way to measure the average dimension of an erythrocyte population, together with its variance (clinically referred as RDW). Such a variation parameter can be easily related to the health status of a patient.

Our results show a valuable approach for the direct light scattering measurement of non-spherical cells. We foresee, on the basis of the results reported in this work, the possibility in the near future to compare between physiological and pathological cell status, opening the scenario of completely label-free diagnostics for blood diseases.

## Notes

<sup>a</sup> Center for Advanced Biomaterials for Healthcare@CRIB, Istituto Italiano di Tecnologia (IIT), Largo Barsanti e Matteucci 53, 80125 Naples, Italy.

<sup>b</sup> Interdisciplinary Research Centre on Biomaterials (CRIB), Università degli Studi di Napoli "Federico II", Piazzale Tecchio 80, 80125 Naples, Italy.

<sup>c</sup> CNR-ISASI Institute of Applied Sciences & Intelligent Systems "E. Caianiello", via Campi Flegrei 34, 80078 Pozzuoli, Italy.

<sup>d</sup> Institut für Werkstofftechnik, Badgasteiner Str. 3, 28359 Bremen, Germany.

<sup>e</sup> Particle and Process Engineering, FB4, University of Bremen, Badgasteiner Str. 3, 28359 Bremen, Germany.

<sup>f</sup> Faculty of Applied Mathematics and Computer Science, Moscow State University, Lenins Hills, 119992 Moscow, Russia.

## References

- 1 M. M. Wintrobe and J. P. Greer, *Wintrobe's clinical hematology*, Wolters Kluwer Health/Lippincott Williams & Wilkins, Philadelphia, 2009.
- 2 L. Miccio, P. Memmolo, F. Merola, P.A. Netti and P. Ferraro, *Nat. Comm.*, 2015, **6**(6502).
- 3 F. Merola, P. Memmolo, L. Miccio, V. Bianco, M. Paturzo and P. Ferraro, *Proc. IEEE*, 2015, **103**(2), 192-204.
- 4 C. B. Black, T. D. Duensing, L. S. Trinkle and R. T. Dunlay, *Assay Drug Dev. Technol.*, 2011, **9**(1), 13-20.
- 5 D. Barnett, B. Walker, A. Landay and T. N. Denny, *Nat. Rev. Microbiol.*, 2008, **6**, S7-S15.
- 6 A. E. Vasdekis and G. Stephanopoulos, *Metab. Eng.*, 2015, **27**, 115-135.
- 7 X. Su, S. E. Kirkwood, M. Gupta, L. Marquez-Curtis, Y. Qiu, A. Janowska-Wieczorek, W. Rozmus and Y. Y. Tsuin, *Opt. Express*, 2011, **19**(1), 387-398.
- 8 P. Memmolo, V. Bianco, F. Merola, L. Miccio, M. Paturzo and P. Ferraro, *IEEE Photon. J.*, 2014, **6**(2), 701106.
- 9 L. Miccio, P. Memmolo, F. Merola, S. Fusco, V. Embrione, A. Paciello, M. Ventre, P.A. Netti and P. Ferraro, *Lab Chip*, 2014, **14**, 1129-1134.
- 10 F. Merola, L. Miccio, P. Memmolo, G. Di Caprio, A. Galli, R. Puglisi, D. Balduzzi, G. Coppola, P. A. Netti and P. Ferraro, *Lab Chip*, 2013, **13**, 4512-4516.
- 11 V. P. Maltsev and K. A. Sem'yanov, *Characterisation of bio-particles from light scattering*. Walter de Gruyter, 2004.
- 12 M. A. Yurkin, K. A. Semyanov, P. A. Tarasov, A. V. Chernyshev, A. G. Hoekstra and V. P. Maltsev, *Appl. Opt.*, 2005, **44**(25), 5249-5256.
- 13 F. Ferri, *Rev. Sci. Instrum.*, 1997, **68**(6), 2265-2274.
- 14 T. F. Wu, Z. Mei and Y. H. Lo, *Lab Chip*, 2012, **12**(19), 3791-3797.
- 15 K. W. Seo, Y. R. Ha and S. J. Lee, *Appl. Phys. Lett.*, 2014, **104**(21), 213702.
- 16 E. J. Lim, T. J. Ober, J. F. Edd, G. H. McKinley and M. Toner, *Lab Chip*, 2012, **12**(12), 2199-2210.
- 17 S. C. Hur, H. T. K. Tse and D. Di Carlo, *Lab Chip*, 2010, **10**(3), 274-280.
- 18 B. S. Lee, Y. U. Lee, H. S. Kim, T. H. Kim, J. Park, J. G. Lee, J. Kim, H. Kim, W. G. Lee and Y. K. Cho, *Lab Chip*, 2011, **11**(1), 70-78.
- 19 T. Wriedt, J. Hellmers, E. Eremina and R. Schuh, *J. Quant. Spectrosc. Radiat. Transf.*, 2006, **100**(1), 444-456.
- 20 J. Q. Lu, P. Yang and X. H. Hu, *J. Biomed. Opt.*, 2005, **10**(2), 024022-02402210.
- 21 M. A. Yurkin and A. G. Hoekstra, *J. Quant. Spectrosc. Radiat. Transf.*, 2011, **112**(13), 2234-2247.

## ARTICLE

- 22 E. Eremina, Y. Eremin and T. Wriedt, *Opt. Commun.*, 2005, **244**(1), 15-23.
- 23 S. V. Tsinopoulos and D. Polyzos, *Appl. Opt.*, 1999, **38**(25), 5499-5510.
- 24 A. M. Nilsson, P. Alsholm, A. Karlsson and S. Andersson-Engels, *Appl. Opt.*, 1998, **37**(13), 2735-2748.
- 25 D. Dannhauser, G. Romeo, F. Causa, I. De Santo and P. A. Netti, *Analyst*, 2014, **139**(20), 5239-5246.
- 26 P. Memmolo, C. Distanto, M. Paturzo, A. Finizio, P. Ferraro and B. Javidi, *Opt. Lett.*, 2011, **36**, 1945-1947.
- 27 P. Memmolo, M. Iannone, M. Ventre, P.A. Netti, A. Finizio, M. Paturzo and P. Ferraro, *Opt. Express*, 2012, **20**, 28485-28493.
- 28 G. Romeo, G. D'Avino, F. Greco, P. A. Netti and P. L. Maffettone, *Lab Chip*, 2013, **13**(14), 2802-2807.
- 29 S. Yang, S. S. Lee, S. W. Ahn, K. Kang, W. Shim, G. Lee, G., K. Hyun and J. M. Kim, *Soft Matter*, 2012, **8**(18), 5011-5019.
- 30 F. Del Giudice, G. D'Avino, F. Greco, I. De Santo, P. A. Netti and P. L. Maffettone, *Lab Chip*, 2015, **15**, 783-792.
- 31 M. Hammer, D. Schweitzer, B. Michel, E. Thamm and A. Kolb, *Appl. Opt.*, 1998, **37**(31), 7410-7418.
- 32 A. N. Shvalov, J. T. Soini, A. V. Chernyshev, P. A. Tarasov, E. Soini and V. P. Maltsev, *Appl. Opt.*, 1999, **38**(1), 230-235.
- 33 Y.C. Fung, W. C. Tsang and P. Patitucci, *Biorheology*, 1981, **18**(3-6), 369.
- 34 P. Memmolo, L. Miccio, F. Merola, O. Gennari, P. A. Netti and P. Ferraro, *Cytometry Part A*, 2014, **85**(12), 1030-1036.
- 35 P. W. Kuchel and E. D. Fackereil, *Bull. Math. Biol.*, 1999, **61**(2), 209-220.
- 36 E. Eremina, J. Hellmers, Y. Eremin and T. Wriedt, *J. Quant. Spectrosc. Radiat. Transf.*, 2006, **102**(1), 3-10.
- 37 K. V. Gilev, E. Eremina, M. A. Yurkin and V. P. Maltsev, *Opt. Express*, 2010, **18**(6), 5681-5690.